ResearchGate

See discussions, stats, and author profiles for this publication at: https://www.researchgate.net/publication/51194809

Effect of Oxidation on Surface-Enhanced Raman Scattering Activity of Silver Nanoparticles: A Quantitative Correlation

ARTICLE *in* ANALYTICAL CHEMISTRY · JUNE 2011

Impact Factor: 5.64 · DOI: 10.1021/ac2005839 · Source: PubMed

CITATIONS
66

READS
140

6 AUTHORS, INCLUDING:

Robert Lupitskyy
University of Louisville
23 PUBLICATIONS **551** CITATIONS
SEE PROFILE

Christopher M Stafford
National Institute of Standards and Technol…
119 PUBLICATIONS **3,817** CITATIONS
SEE PROFILE

Henry Du
Stevens Institute of Technology
119 PUBLICATIONS **1,523** CITATIONS
SEE PROFILE

Svetlana Sukhishvili
Stevens Institute of Technology
134 PUBLICATIONS **4,812** CITATIONS
SEE PROFILE

Available from: Robert Lupitskyy
Retrieved on: 30 January 2016

analytical chemistry

ARTICLE

pubs.acs.org/ac

Effect of Oxidation on Surface-Enhanced Raman Scattering Activity of Silver Nanoparticles: A Quantitative Correlation

Yun Han,[†] Robert Lupitskyy,[‡] Tseng-Ming Chou,[†] Christopher M. Stafford,[§] Henry Du,*[,†] and Svetlana Sukhishvili*[,‡]

[†]Department of Chemical Engineering and Materials Science and [‡]Department of Chemistry, Chemical Biology and Biomedical Engineering, Stevens Institute of Technology, Castle Point on Hudson, Hoboken, New Jersey 07030, United States

[§]Polymers Division, National Institute of Standards and Technology, Gaithersburg, Maryland 20899, United States

Supporting Information

ABSTRACT: We quantitatively studied, using X-ray photoelectron spectroscopy (XPS), oxidation of substrate-immobilized silver nanoparticles (Ag NPs) in a wide range of conditions, including exposure to ambient air and controlled ozone environment under UV irradiation, and we correlated the degree of silver oxidation with surface-enhanced Raman scattering (SERS) enhancement factors (EFs). The SERS activity of pristine and oxidized Ag NPs was assessed by use of *trans*-1,2-bis(4-pyridyl)ethylene (BPE) and sodium thiocynate as model analytes at the excitation wavelength of 532 nm. Our study showed that the exposure of Ag NPs to parts per million (ppm) level concentrations of ozone led to the formation of Ag_2O and orders of magnitude reduction in SERS EFs. Such an adverse effect was also notable upon exposure of Ag NPs under ambient conditions where ozone existed at parts per billion (ppb) level. The correlated XPS and SERS studies suggested that formation of just a submonolayer of Ag_2O was sufficient to decrease markedly the SERS EF of Ag NPs. In addition, studies of changes in plasmon absorption bands pointed to the chemical enhancement as a major reason for deterioration of SERS signals when substrates were pre-exposed to ambient air, and to a combination of changes in chemical and electromagnetic enhancements in the case of substrate pre-exposure to elevated ozone concentrations. Finally, we also found UV irradiation and ozone had a synergistic effect on silver oxidation and thus a detrimental effect on SERS enhancement of Ag NPs and that such oxidation effects were analyte-dependent, as a result of inherent differences in chemical enhancements and molecular binding affinities for various analytes.

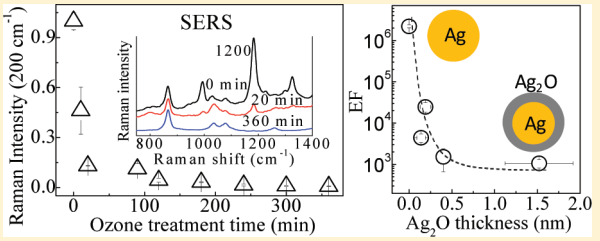

Surface-enhanced Raman scattering (SERS) is an attractive analytical technique for label-free detection and identification of chemical and biological species at trace concentrations.[1−3] While significant advances have been made in engineering various SERS-active metal (mainly Ag and Au) nanostructures,[4−13] SERS is far from being adopted as a routine analytical technique. This is mainly due to the strong dependence of SERS enhancement on structural, morphological features of metal nanostructures[13−20] as well as on surface chemistry and details of molecular binding. Significant challenges remain, in particular, when Ag, often a metal of choice because of its inherently higher SERS activity compared to its Au counterpart, is used in preparation of SERS-active nanostructures. Silver is prone to oxidation even under ambient conditions, and this results in significant changes in the chemical and plasmonic properties of Ag nanoparticles (Ag NPs).[21−25] For example, exposure to air or oxygen has been reported to cause a red shift of Ag NP plasmonic bands[21,23,24] Another example is an interesting observation of the dependence of oxidation of Ag NPs on the NP size.[22,26] In this report, we aim to identify and quantify surface oxidation species using X-ray photoelectron spectroscopy (XPS) and to demonstrate their effect on SERS activity of Ag NPs.

The effects of oxidation on SERS activity of Ag nanostructures are far from being understood, and experimental reports are both rare and fragmented. In one earlier study of cryogenically deposited (32 K) porous silver film, Raman signals from ethylene and pyridine adsorbed at porous silver film were quenched upon exposure to small amounts of oxygen (approximately 0.1 monolayer).[27] This effect was hypothetically attributed to dissociative adsorption of oxygen at SERS active sites of silver surface and changes in the chemical component of the SERS enhancement. Recently, we have demonstrated that exposure of SERS substrates with immobilized Ag NPs synthesized in Ar to the lab ambient environment was sufficient to result in 5 orders of magnitude penalty in the detection limit for nitroaromatic molecules in aqueous solutions.[28] Qi et al.[26] reported similar observations regarding the instability of Ag NPs in air.

While oxidation of Ag nanostructures has previously been shown to decrease their SERS activity, here we have revealed the chemical identity of oxidized surface species (different forms of Ag oxides), quantified their amounts, and for the first time established quantitative correlations between the degree of Ag NP oxidation and SERS enhancement factors (EFs). Our studies

Received: March 5, 2011
Accepted: June 6, 2011
Published: June 06, 2011

 © 2011 American Chemical Society dx.doi.org/10.1021/ac2005839 | *Anal. Chem.* 2011, 83, 5873–5880

embrace a wide range of environmental conditions, starting from ambient ones (situation usually met during analytical SERS-based sensing) to environments with enhanced and controlled concentrations of an oxidizing species (ozone). Simultaneous observations of plasmonic and chemical changes during Ag NP oxidation, and correlating these changes with Ag NP SERS performance, allowed us to understand the relative importance of chemical and electromagnetic mechanisms in SERS quenching at various stages of Ag NP preoxidation. Interestingly, while SERS EFs dropped dramatically upon long-term (days) exposure of Ag NPs to ambient air, we found neither evidence of formation of silver oxide at the surface nor significant changes in Ag NP plasmon bands (factors pointing to changes in SERS chemical enhancement at this time scale). At controlled higher levels of ozone content (~17 ppm), growth of Ag_2O occurred, resulting in a sharp degradation of SERS activity due to a simultaneous decrease in chemical and electromagnetic enhancements. Finally, at concentrations of ozone $\gg$20 ppm, Ag_2O was converted to AgO, and the SERS signals were completely degraded.

Moreover, seeking to imitate SERS measurements outdoors when substrates are exposed to sunlight, we studied the combined effect of ozone and UV−vis light exposure on oxidation and SERS performance of Ag NP-based substrates, and we also explored how Ag NP preoxidation affects the SERS activity toward various analyte molecules. Our study contributes strongly to the understanding of plasmonic and molecular consequences of Ag NP oxidation on their SERS enhancement. The results and conclusions will be useful for the development of stable and reproducible SERS substrates for ultrasensitive chemical and biological sensing.

EXPERIMENTAL SECTION

General. Equipment and instruments or materials are identified in the paper in order to adequately specify the experimental details. Such identification does not imply recommendation by the National Institute of Standards and Technology (NIST), nor does it imply the materials are necessarily the best available for the purpose.

Materials. All chemical reagents were purchased from the indicated suppliers and used without further purification: sodium citrate dehydrate (enzyme grade, Fisher), silver nitrate (ultrapure grade, Acros), $HAuCl_4$ solution (99.99% trace metals basis, 30 mass % by mass in dilute HCl, Aldrich), sodium thiocyanate (NaSCN, 99.99%, Aldrich), *trans*-1,2-bis(4-pyridyl)ethylene (BPE; 97%, Aldrich), poly(allylamine hydrochloride) (PAH; mass-average molecular mass M_w of 15 000 g/mol, Aldrich), and ethanol (anhydrous, 99.8%, Aldrich). Water used for experiments was filtered with Barnstead ion-exchange columns and then further purified by passage through Millipore (Milli-Q) columns. All glassware and substrates were cleaned in Nochromix (Godax Laboratories, Inc.) solution in concentrated sulfuric acid overnight, followed by thorough rinsing with Milli-Q water.

Synthesis of Ag and Au NPs. Ag NPs were synthesized by a modified Lee and Meisel procedure.[4] $AgNO_3$ (424 μL of 100 mM solution) was diluted in 39.576 mL of water to give a 1 mM $AgNO_3$ solution. Sodium citrate (0.8 mL of 1% by mass solution in water) was then added dropwise into the $AgNO_3$ solution under continuous stirring. The mixture was stirred for approximately 1 min and then transferred into a UV chamber (UV flood curing system, cure zone 2; CON-TROL-CURE, Chicago, IL). A water bath was used to keep the reaction mixture between 25 and 50 °C. The bath water was changed every half hour. The chosen temperature interval assured fast growth of relatively monodispersed, spherically shaped Ag NPs. The reaction mixture was kept under UV irradiation with continuous stirring for 2 h in an argon-filled glovebox. The resultant Ag colloidal solution was orange-brown in color. The colloidal solution was wrapped in aluminum foil to avoid light exposure and stored in the argon-filled glovebox. The ζ-potential of produced Ag colloids measured on a Zetasizer Nano-ZS (Malvern Instruments, Inc.) was −40 mV ± 5 mV in Milli-Q water. The average particle diameter of the Ag colloids characterized by Zetasizer was 48 nm with a polydispersity index of 0.12. Moreover, transmission electron microscopy (TEM; data not shown) and scanning electron microscopy (SEM) measurements (see, for example, Figure 1) were used to further confirm the size of synthesized Ag NPs. The results from different techniques are consistent. UV−visible absorption spectrum of Ag nanoparticle solution obtained with the Synergy HT multidetection microplate reader (BioTek Instruments) showed an absorbance peak at 410 nm with full width at half-mazimum (fwhm) ~60 nm. These results indicate a narrower Ag NP size distribution when compared to Ag NPs produced by the Lee and Meisel reduction method.

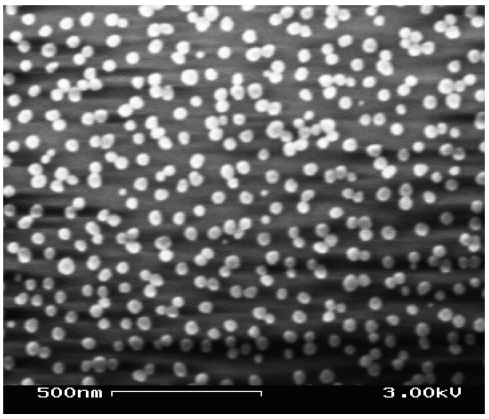

Figure 1. SEM image of Ag NPs synthesized in argon environment and immobilized on a glass slide with PAH as an anchoring layer by 24 h deposition from 10^{12} particle/mL solution at pH 5.6.

Au NPs were synthesized by mixing 20 mL of $HAuCl_4$ (4 mM) and 20 mL of citrate (6.24 mM) and exposing the mixture to UV light for 30 min, otherwise following the same procedure of Ag nanoparticle synthesis. The resultant gold colloids were reddish in color with a plasmonic absorption peak at 550 nm. The average size of the resultant gold nanoparticles was 80 nm with a polydispersity index of 0.16 and ζ-potential 38 mV ± 5 mV in Milli-Q water. The colloidal solution was protected with aluminum foil to avoid light exposure and stored in the argon-filled glovebox.

Preparation of SERS Substrates and XPS Samples. SERS substrates were prepared by immobilizing Ag or Au NPs on the bottom of homemade glass cells following the detailed procedure described earlier.[28] Glass cells were filled with 1 M NaOH for 5 min to increase the negative charge on the glass surface and then rinsed thoroughly with Milli-Q water. They were then filled with 0.2 mg/mL PAH solution, the pH was adjusted to 9 for 30 min, and the glass cells were rinsed thoroughly with Milli-Q water. From ellipsometric measurements, the thickness of dry monolayers of adsorbed PAH was ~9 Å. Finally, PAH-coated glass cells were filled with Ag colloidal solution for 24 h, then rinsed with argon-purged Milli-Q water, and kept full with argon-purged Milli-Q water. SERS substrates were prepared and stored in the argon-filled glovebox.

For the preparation of XPS samples, silicon wafers were precoated with a 90 nm thick gold film by atomic layer deposition to eliminate oxygen contribution from native oxide during XPS analysis. Ag NPs were then immobilized onto silicon wafers following the same procedure as that for SERS substrate preparation.

Oxidative Treatment of SERS and XPS Samples. Oxidation of Ag NPs with controlled ozone concentration was performed by use of an Air-Duct 2000 ozone generator (Air-Zone Inc., Suffolk, VA). Oxygen flow was used to maintain ozone concentration at 17 ± 1 ppm level. Ozone concentration was measured via OS-4 Ozone Switch sensor (Eco Sensors, Inc.) with a detection range from 10 ppb to 20 ppm. UV exposure was performed in a Cure Zone 2 UV flood curing system (CON-TROL-CURE, Chicago, IL) with a 400 W metal halide lamp as a source of UV irradiation (spectral range 320−400 nm). The intensity of the UV irradiation was 80 mW/cm^2 at a distance of 5 cm from the protective shield of the lamp. The samples were placed 22.5 cm from the protective shield of the UV lamp.

Oxidation at high ozone concentration was performed by use of a mercury UV grid lamp (BHK Inc., Claremont, CA) with a 185 nm ozone-producing band. The intensity of the UV light was 7.5 mW/cm^2 at 2.5 in. from the lamp. The ozone level generated by this lamp (≫20 ppm) was beyond the detection limit of our ozone sensor. Samples were placed 10 cm from the lamp for oxidation treatment.

SERS and XPS Measurements. SERS setup and measurements were described in our earlier publication.[28] SERS signal was collected by use of an Olympus 40× objective, N.A. 0.85, with the laser beam probing the surface-immobilized Ag NPs through the transparent glass substrate adhesively bonded to one end of precut glass tubes to form a watertight sample cell for in situ measurements. The cell was filled with 400 μL of an analyte solution at its bottom prior to SERS measurements. In this work SERS measurements were performed at the excitation wavelength of 532 nm and the power of 2.8 mW for Ag NPs and at 633 nm and 3.7 mW for Au NPs. While typical spectra were collected for 10 × 20 s, at this laser power the SERS features were not affected by illumination time, and similar results were obtained when spectra were collected via 20 × 1 s exposure. Nikon 20× 0.4 N/A objective was used to produce a large laser focusing beam (~1 mm in diameter). These large, defocused excitation spots, as well as the uniform Ag NP coverage density, resulted in a relatively small, <15% spot-to-spot variation in SERS intensity. Measurements were performed in three different spots of each substrate and averaged. Data were processed with Grams32 v5 and Origin 7.5 software.

A Kratos Axis Ultra DLD X-ray photoelectron spectrometer with monochromatic Al K_α X-rays was used to determine the oxidation state of the Ag NPs. Samples were removed from Ar storage, mounted on a sample holder, and quickly installed into the load lock to minimize air exposure. Scans at spectral resolution 0.1 eV were collected at 20 eV pass energy for the Ag 3d, Au 4f, C 1s, and O 1s regions at three separate locations on each sample. A low-energy electron flood gun was used to minimize charging. All peaks were corrected by referencing the primary peak of the Au 4f signal at 84.0 eV. XPS data were processed with CasaXPS and Origin 7.5 software.

RESULTS AND DISCUSSION

Because of our focus on quantifying the effect of Ag NP oxidation on their SERS activity, it was important that Ag NPs were synthesized in an argon environment. To avoid environmental oxidation of as-synthesized Ag NPs during their immobilization on PAH-modified, gold-coated silicon wafers (for XPS only) or glass slides (for SERS studies), NP surface immobilization was also performed in an argon-filled glovebox. Figure 1 shows a typical SEM image of immobilized Ag NPs at a dense particle coverage containing 19 ± 1 dimers, 6 ± 1 trimers, and 3 ± 1 larger aggregates per square micrometer. These aggregates included ~69% of the total number of surface-immobilized Ag NPs and served as SERS "hot spots" in SERS measurements, contributing to the majority of the SERS signal.[2,29] Here, we followed a line of thought that molecular oxygen does not oxidize silver under ambient conditions[30,31] and ozone is considered as the primary oxidant that initiates the process of silver oxidation,[26,28,32,33] and we aimed to monitor and control the ozone content during substrate oxidative pretreatment. The concentration of ozone in our experiments varied from 250 to 400 ppb in ambient air and was also controlled at the mild level of 17 ± 1 ppm in order to establish quantitative correlation between the degree of Ag NP oxidation (probed by XPS) and SERS performance of Ag NP-immobilized substrates. In addition, the effect of higher ozone concentrations ≫20 ppm on Ag NP SERS activity was also investigated.

Quantitative Correlation of Oxidation of Ag NPs with Their SERS Activity. For XPS and SERS experiments described in this section, dry substrates containing immobilized unoxidized Ag NPs were simultaneously exposed to ozone at 17 ± 1 ppm and UV irradiation. These substrates were then either analyzed by XPS to determine the silver oxide formation, or exposed to analyte solutions for SERS measurements. Figure 2 shows (a) high-resolution Ag 3d spectra and (b) binding energies of Ag 3d peaks. The Ag 3d binding energy of 368.15 eV for the unoxidized sample is close to the value reported for metallic Ag.[34,35] Samples oxidized for 180, 240, 300, and 360 min have a significant ~0.3 eV shift in the Ag 3d peak position to lower binding energies. There is no significant difference, however, between Ag 3d binding energies of oxidized samples. Corresponding Ag 3d peak positions are within the uncertainty of the measurement (~0.1 eV). Unlike other metals, silver exhibits a yet-to-be-explained shift to lower binding energy as the oxidation state of Ag occurs. According to the literature, the shift is usually smaller for Ag_2O (0.3−0.4 eV) and larger for AgO (0.8−1.0 eV).[30,36] The direction and magnitude of the Ag 3d peak shift in our case suggests the formation of Ag_2O. Additionally, formation of silver oxidation on Ag NPs was also confirmed by energy-dispersive X-ray spectroscopy (EDS), as shown in Figure S-1, Supporting Information.

Spectral changes in the O 1s region of XPS spectra provided more quantitative information on the kinetics of Ag_2O formation. High-resolution spectra of O 1s obtained from the samples oxidized for 0, 180, and 360 min are presented in Figure 3a. The O1s spectra are broad and complex, suggesting contributions of several oxygen species. A peak at 530.6 eV is attributed to Ag_2CO_3 and adsorbed CO_2 (530.5−531.0 eV).[30,37] A broad peak at 531.9−532.0 eV is associated with dissolved oxygen (530.5−531.5 eV),[38,39] as well as oxygen originating from citrate molecules or products of citrate oxidation.[40] A change in the relative intensities of these two peaks after longer oxidation treatment time can be attributed to the oxidation of the organic layer around Ag NPs. Starting from 180 min of exposure to the oxidative environment; a shoulder appears at 529.1 eV. The intensity of the shoulder grows with treatment time. The position of the shoulder agrees well with the literature data for the O 1s binding energy for Ag_2O (529.5 eV for lightly oxidized silver surface and 529.2 eV for bulk Ag_2O have been reported).[30] The O 1s spectra were curve-fitted and Ag_2O peak fraction was plotted as a function of oxidation time in Figure 3b.

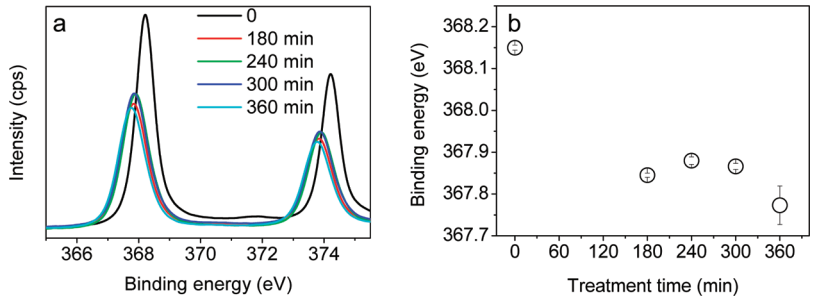

Figure 2. (a) High-resolution Ag 3d X-ray photoelectron spectra and (b) average Ag $3d_{5/2}$ peak position from Ag NP substrates treated for 0, 180, 240, 300, and 360 min with ozone (17 ± 1 ppm) and UV (320−400 nm). Error bars indicate one standard deviation of the data as calculated from measurements taken at three different spots of the sample, which is taken as the uncertainty of the measurement.

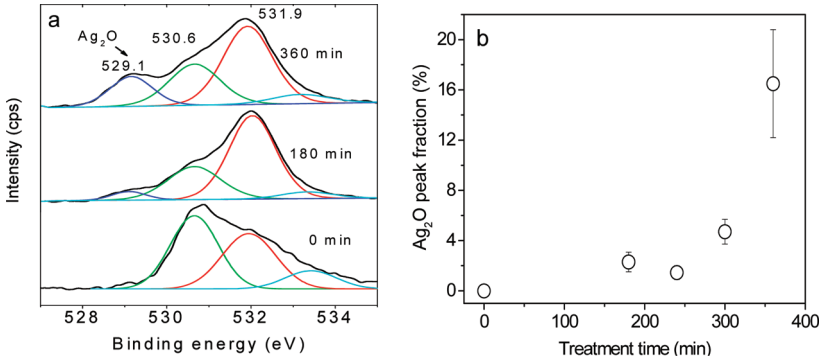

Figure 3. (a) High-resolution O 1s X-ray photoelectron spectra from Ag NPs treated for 0, 180, and 360 min with ozone (17 ± 1 ppm) and UV. (b) Percentage area of Ag_2O in O 1s spectra as a function of treatment time. Error bars indicate one standard deviation of the data as calculated from measurements taken at three different spots of the sample, which is taken as the uncertainty of the measurement.

We made an estimate of the thickness of the Ag_2O layer formed based on the atomic percentages of Ag, C, and O, as determined by the XPS CASA software. An assumption was made that we have a flat, stratified layer consisting of silver, silver oxide, and carbon. Oxygen atoms other than those from silver oxide are evenly distributed within carbon and silver layers. We also assume that the layer is homogeneous and contains no voids. The layer thickness is taken to be equal to the penetration depth of X-rays at 90° takeoff angle (8.5 ± 1.5 nm) and the atomic densities of the components are assumed to be the same. This way, the thickness of the silver(I) oxide formed after 360 min of treatment was estimated to be 1.5 ± 0.4 nm, which shows that we are dealing with very thin oxide layers. Given the assumptions of a homogeneous and continuous layer, this number should be taken as a rough estimate.

We then aimed to correlate the estimated thickness of Ag_2O with SERS activity of preoxidized substrates containing immobilized Ag NPs. We used charge-neutral *trans*-1,2-bis(4-pyridyl)ethylene (BPE) in ethanol as a model analyte. In all cases, oxidation treatment of Ag NP substrates was done prior to the addition of the analyte. SERS measurements were performed in analyte solutions as opposed to "dry" measurements, which are often used in SERS studies.[41−45] Figure 4a shows SERS intensities of 1 ppm BPE at 1200 cm^{-1} as a function of oxidation treatment time (SERS intensities from preoxidized substrates were normalized to the intensity measured with nonoxidized substrates). SERS intensity decreased rapidly, especially during the first hour of exposure. Figure 4b shows the evolution, as a function of substrate oxidation time, of surface plasmonic resonance (SPR) spectra of substrate-immobilized Ag NPs. The 395 nm band is associated with absorption of isolated Ag NPs and also contains a partial contribution from the transverse plasmon mode of aggregated Ag NPs,[42,4345,46] while a second broad peak at 720 nm is mainly associated with longitudinal mode of plasmon coupling within Ag NP aggregates. Oxidative treatment (20 min) with ozone and UV resulted in broadening and a red shift of the 395 nm band (Figure 4b). This effect progressed at 3 h of oxidation treatment and slowed down at longer oxidation times. This result agrees with previous reports on the effect of oxidation of Ag NPs on plasmonic properties of individual Ag colloids in solution.[21,24] At the same time, SEM measurements of immobilized Ag NPs indicated no change in the distribution of Ag NPs within surface aggregates after 6-h oxidation treatment, as shown in the inset in Figure 4 b (compare to Figure 1). Taken together, these data suggest that a decrease in SERS activity of immobilized Ag NPs (Figure 4 a) occurred through a combined decrease in chemical and electromagnetic components of SERS enhancement.

According to the chemical enhancement mechanism, a charge transfer occurs between the metal and adsorbate at the sites of atomic-scale roughness.[47,48] It is usually considered that charge transfer can contribute up to several orders of magnitude to the overall surface enhancement value. In this model, the incident photon excites a charge-transfer process between the Fermi level of the metal adatoms (surface defect sites) and adsorbate levels that become accessible in energy upon interaction of the adsorbate with the metal surface.[49] This mechanism can be applied especially at the early stages of silver oxide formation. For charge transfer between the adsorbate and the metal to be quenched, the vacant Ag levels at these specific defect sites must

dx.doi.org/10.1021/ac2005839 |*Anal. Chem.* 2011, 83, 5873–5880

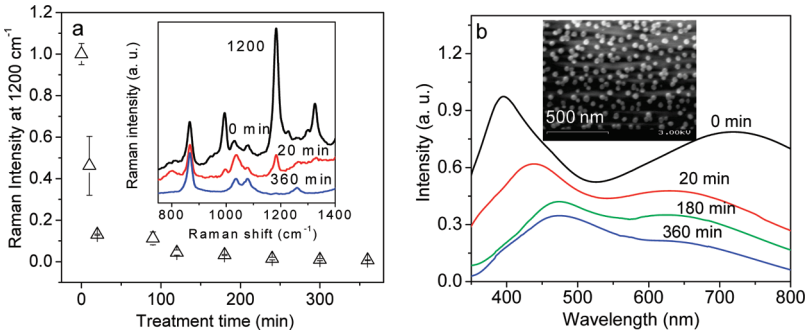

Figure 4. (a) Normalized SERS intensity of 1 ppm BPE in ethanol at 1200 cm^{-1} as a function of oxidation time of Ag NPs. (Inset) SERS spectra of 1 ppm BPE in ethanol at the surface of immobilized Ag NPs treated for 0, 20, and 360 min with ozone (17 ± 1 ppm) and UV. Spectra were acquired with 2.8 mW laser power at 532 nm excitation with 20 s acquisition time. Intensities were normalized to intensities measured with corresponding unoxidized substrates. Error bars indicate standard deviation of the data as calculated from measurements taken at three different spots of the sample, which is taken as the uncertainty of the measurement. Because of the statistical uniformity of aggregated Ag NPs within the defocused beam (~1 mm in diameter) SERS probing area, the spot-to-spot of SERS signal variation was less than 15%. (b) Surface plasmon resonance (SPR) absorption of SERS substrates (immobilized Ag NPs) treated with ozone (17 ± 1 ppm) and UV for various time periods. (Inset) SEM image of immobilized Ag NPs after 6-h oxidation treatment.

be altered in energy so that the incident radiation is no longer in resonance with the energy difference between these levels. Overlayer atoms fill vacant levels at the defect sites, thereby raising the Fermi energy at these sites. Another significant component in SERS activity is electromagnetic enhancement, usually considered as a major contributor to SERS, which provides an EF from 10^6 to 10^{11}.[50,51] The electromagnetic model of the surface enhancement developed by Murray,[52] for example, considers that the deposition of an overlayer may increase the imaginary part of the macroscopic surface dielectric function,[53,54] leading to a decrease in electromagnetic field and SERS enhancement. In our case, the formation of Ag oxide increases the dielectric constant of Ag NPs, causing red shift and a decrease in intensities of plasmonic bands.[46]

We further aimed to establish quantitatively how the SERS enhancement factor (EF) is affected by oxidation of Ag NPs (Figure 5). EFs were calculated for BPE in ethanol by use of the 1200 cm^{-1} band according to eq 1 with integrated intensities of the characteristic bands:

$$\mathrm{EF} = \frac{\dfrac{I_{\mathrm{SERS}}}{C_{\mathrm{SERS}}}}{\dfrac{I_{\mathrm{NR}}}{C_{\mathrm{NR}}}} \qquad (1)$$

where I_{SERS}, C_{SERS} and I_{NR}, C_{NR} are integrated Raman intensities and concentrations of analytes in solutions used in SERS and normal Raman measurements, respectively. This analytical method is fairly intuitive and provides a simple means to compare SERS efficiencies of various substrates without making specific assumptions about the surface densities of SERS-active sites and/or the surface density of adsorbed molecules.[55] An illustration of EF calculation is provided in the Supporting Information. Note that SERS data used in EF calculation were obtained at the analyte concentration of detection limit. Figure 5 correlates the estimated Ag_2O thickness with SERS EF. As shown in the graph, in the early stage of oxidation on Ag NP surface, SERS EF drops sharply with increasing Ag_2O thickness. Up to 3 orders of magnitude decrease in SERS EF compared to that for unoxidized Ag NPs has been observed when only ~0.4 nm thick Ag_2O formed on Ag NPs. In the later stage of silver oxidation, further increase in Ag_2O thickness causes an additional yet smaller decrease in SERS EF.

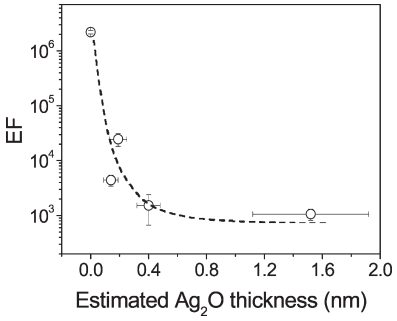

Figure 5. Correlation between EFs calculated for BPE in ethanol and estimated thickness of Ag_2O (from data in Figure 3). Error bars indicate one standard deviation of the data as calculated from measurements taken at three different spots of the sample, which is taken as the uncertainty of the measurement.

Analyte-Dependent Effect of Oxidation. We have also explored the effect of Ag NP oxidation on SERS activity using a different analyte, NaSCN. SCN^- is a common anionic analyte with high affinity to the silver surface. It has a pronounced band at 2108 cm^{-1}, corresponding to C−N stretching vibration. As shown in Figure 6a, SERS intensity of 2108 cm^{-1} from 1 ppm SCN^- in water decreased when immobilized Ag NPs were oxidized by exposure to ozone and UV irradiation, similar to our observation with BPE. However, compared with BPE, a decrease in SERS activity of SCN^- was significantly smaller after the same oxidation treatment of Ag NPs, as shown in Figure 6b. This distinct behavior of the analytes is especially dramatic during the first hour of oxidative exposure, suggesting that BPE is more sensitive to the oxidation of Ag NPs than SCN^-.

Analyte dependence of SERS sensitivity to silver oxidation can be attributed to two factors. The first factor is different effects of Ag NP oxidation on the binding strength of various analytes. The affinity of BPE for Ag NP surface diminishes more dramatically as a result of oxidation than the affinity of SCN^-, because of stronger binding of SCN^- with the surface of silver. Stronger binding SCN^- ions may displace silver oxide from the thin layer of silver oxide to form AgSCN, which still contributes to SERS of SCN^-. The second factor for the difference could be accounted for by changes in the chemical contribution to SERS EFs. This can be attributed to different energies

dx.doi.org/10.1021/ac2005839 |Anal. Chem. 2011, 83, 5873–5880

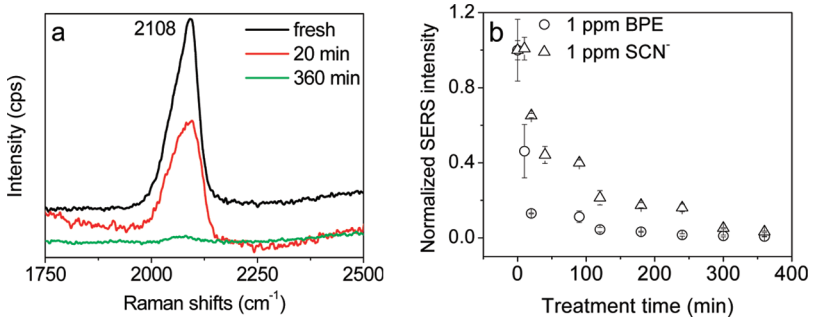

Figure 6. (a) SERS spectra of 1 ppm SCN^- in water at the surface of immobilized Ag NPs treated for 0, 20, and 360 min with ozone and UV. (b) Normalized SERS intensity of (○) 1 ppm BPE in ethanol at 1200 cm^{-1} and (△) 1 ppm SCN^- in water at 2108 cm^{-1} as a function of oxidation time of Ag NPs. Spectra were acquired with 2.8 mW laser power at 532 nm excitation with 20 s acquisition time. Error bars indicate one standard deviation of the data as calculated from measurements taken at three different spots of the sample, which is taken as the uncertainty of the measurement.

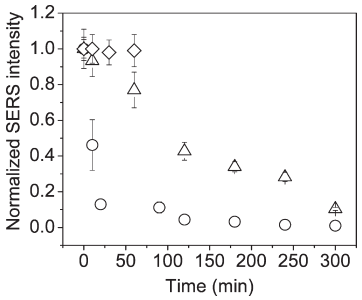

Figure 7. Normalized SERS intensity of 1 ppm BPE in ethanol at 1200 cm^{-1} as a function of oxidation time from Ag NPs exposed (△) to ozone only, (◇) to UV only, and (○) to a combination of ozone and UV. Error bars indicate one standard deviation of the data as calculated from measurements taken at three different spots of the sample, which is taken as the uncertainty of the measurement.

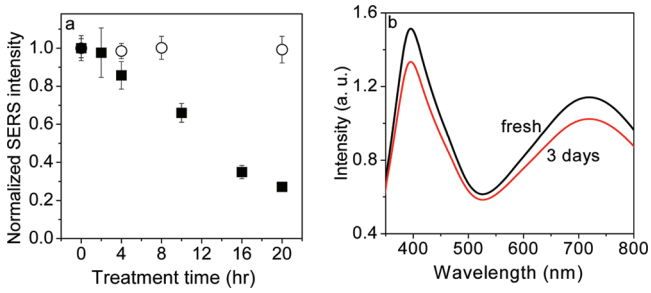

Figure 8. (a) SERS intensity of 1 ppm BPE in ethanol at 1200 cm^{-1} as a function of exposure time with (■) Ag NPs and (○) Au NPs exposed to environmental ozone and sunlight, and (b) UV−vis absorption spectra of SERS substrates (immobilized Ag NPs) freshly prepared without oxidation and exposed to ambient air for 3 days. Error bars indicate one standard deviation of the data as calculated from measurements taken at three different spots of the sample, which is taken as the uncertainty of the measurement.

of the electron levels that participated in charge transfer in the case of adsorbed BPE and SCN^- analytes. Upon adsorption of oxygen atoms, the Fermi levels at the defect sites increase in their energy.[49] Therefore, BPE, probably having lower than SCN^- electron levels participating in the charge transfer, requires lower degrees of surface oxidation to move the charge transfer to the Fermi level out of resonance with the incident radiation.

Synergistic Effect of Ozone and UV. Since silver(I) oxide is known to be a photosensitive semiconductor,[56] electromagnetic radiation is expected to promote Ag NP oxidation. Here, we directly demonstrate the effect of such a synergistic oxidation on SERS performance of Ag NPs achieved by the use of ozone in combination with UV irradiation. As a reference, we conducted experiments where the samples were exposed to ozone only and to UV only in the absence of oxygen. SERS measurements were performed with 1 ppm solution of BPE in ethanol as an analyte. As seen in Figure 7, SERS intensities from the samples treated by UV only up to 60 min remain the same as the initial one from untreated sample, suggesting no oxidation occurred when Ag NPs were exposed to UV light without oxygen in the environment. As compared to samples treated with ozone only, SERS intensities decreased much more dramatically for the samples treated with a combination of ozone and UV irradiation. This can be explained through the surface charge-transfer photochemistry.[57] The surface plasmonic absorption band of Ag NPs is on the edge of the UV source spectrum (320−400 nm) used in the experiment. Silver surface electrons, excited by the UV irradiation, are transferred to the adsorbed O_3 molecules, increasing dissociative sticking probability and facilitating oxidation of silver atoms. For nanoparticles, the electric field building up upon ionization of adsorbed oxygen atoms on Ag surface is the driving force of the oxide growth.[58] Because of the photosensitive semiconducting properties of Ag_2O,[56] UV irradiation promotes electron tunneling from the metal−oxide interface to the adsorbed oxygen, leading to ionization of the oxygen atoms and an increase in the oxidation driving force.

Oxidation of Silver by Atmospheric Ozone. We then sought to assess the effect of outdoor exposure on SERS activity of silver substrates. SERS cells with immobilized NPs were covered with a quartz slide in a way that prevents contamination by dust yet allows free air to penetrate inside. The samples were exposed for up to 20 h outdoors. Ambient ozone concentrations varied depending on the location and weather conditions. Our experiments were performed on sunny days of the summer with measured ozone concentration of 250−400 ppb. This concentration was 50−100 times lower than the ozone concentration used in our laboratory experiments with ~17 ppm ozone concentration shown in Figures 4−7. The SERS measurements were performed with BPE as an analyte. Ag NPs showed a 3-fold decrease in EF as a result of the outdoor exposure, as shown in Figure 8(■). The formation of Ag_2O layer under such mild oxidative conditions, however, could not be detected by XPS after 20 h of exposure time. The lack of detectable Ag_2O was also confirmed by the UV−vis data that showed no significant shift in

dx.doi.org/10.1021/ac2005839 |Anal. Chem. 2011, 83, 5873–5880

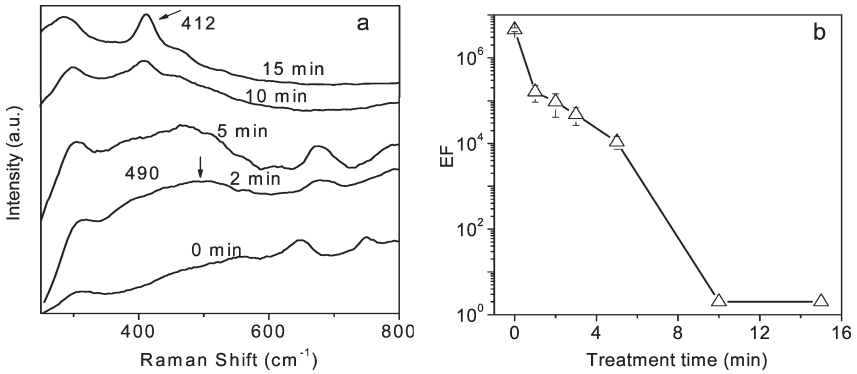

Figure 9. (a) SERS spectra of immobilized Ag NPs after different treatment time periods and (b) corresponding SERS EFs as a function of oxidation duration. Ozone concentration, ≫ 20 ppm; UV source, mercury lamp (185−400 nm). Spectra were acquired with 2.8 mW laser power at 532 nm excitation with 20 s acquisition time. Error bars indicate one standard deviation of the data as calculated from measurements taken at three different spots of the sample, which is taken as the uncertainty of the measurement.

the surface plasmon bands of immobilized Ag NPs after 3-day exposure to environmental air (Figure 8b). Note that, unlike the data reported by Qi et al.,[26] we are reporting here a short-term effect of exposure of Ag NP to air, and all samples were pre-exposed to air for a 1-min duration. Importantly, control experiments with SERS samples kept in a nitrogen-filled glovebox in either dry or wet state for over a week showed no decrease in SERS activity for BPE. Moreover, no deterioration of SERS signal was observed when SERS substrates were exposed to light in a nitrogen atmosphere. We suggest that chemisorbed oxygen might be responsible for the decrease of the Raman signal in Figure 8a, mostly due to a decrease in chemical enhancement and/or decreased binding of the BPE molecules to the surface of Ag NPs. In contrast, similar experiments with immobilized Au NPs did not demonstrate changes in the NP SERS activity (Figure 8, ○), linking high oxidative stability of Au NPs with their consistent SERS performance.

Oxidation of Ag NPs at High Ozone Concentration. Although we have successfully detected and quantified the formation of Ag_2O at 17 ± 1 ppm ozone concentration, using XPS, we were not able to detect Ag−O stretching vibrations at 490 cm^{-1} [30] in SERS experiments, likely due to both low Raman activity and the small amount of Ag_2O formed at this moderate ozone concentration. Therefore, oxidation of Ag NPs was conducted at a much higher ozone concentration of ≫20 ppm (see Experimental Section).

Figure 9a shows SERS spectra of immobilized Ag NPs oxidized for different amounts of time, which were collected in the absence of analyte. A broad Raman peak at 490 cm^{-1} associated with Ag−O stretching vibrations in Ag_2O[30] emerges after 1−2 min of such a severe oxidative treatment. The intensity of this peak decreases after 5 min of exposure, giving rise to another peak at ∼412 cm^{-1}, attributed to Ag−O stretching vibrations in AgO. After 15 min of oxidation treatment, a drastic change in particle morphology and full conversion from metallic Ag to AgO occurred, as indicated by high-resolution TEM and X-ray diffraction (XRD) spectroscopy (Figure S-2, Supporting Information). Figure 9b shows SERS EFs acquired with Ag NP substrates as a function of the oxidation time in these severe conditions. EFs calculated from integrated intensities of 1608 and 1639 cm^{-1} SERS bands obtained with 100 ppb BPE solutions brought in contact with oxidized silver NP substrates (Figure S-3, Supporting Information) decreased with oxidation time and fell virtually to zero with 10-min preoxidized substrates, when Ag was almost completely converted to AgO.

CONCLUSIONS

Our systematic oxidation treatment of Ag NPs immobilized on planar substrates coupled with detailed analytical examination and SERS measurements have led us to correlate quantitatively the extent of oxidation with SERS EFs of Ag NPs. Particularly, the SERS EF significantly drops when pristine Ag NPs undergo even a mild degree of oxidation in the form of only submonolayer Ag_2O coverage on Ag NPs. At this stage of NP oxidation, the decrease in SERS activity of Ag NPs can be attributed primarily to decreased adsorption of the analyte and changes in chemical contribution to SERS enhancement. However, at the later stage of oxidation, changes in EFs originate from a combined effect of chemical and electromagnetic components of the SERS enhancement. In addition, the effect of oxidation of Ag NPs on their SERS performance was dependent on the nature of the analyte, due to different chemical enhancement features, as well as varied molecular binding strength to the silver surface. These findings will serve as an important reminder regarding the complexity of the SERS phenomenon. Furthermore, they will form a valuable knowledge base for the development of stable and reproducible SERS platforms for chemical and biological sensing in the real world.

ASSOCIATED CONTENT

Supporting Information. Additional text and three figures, showing SEM images and EDS maps of Ag and O of Ag NPs unoxidized and treated for 6 h with ozone and UV; TEM images and XRD spectra of Ag NPs before and after treatment at high ozone concentration; and SERS spectra of BPE acquired with Ag NP substrates treated at high ozone concentration for various time periods. This material is available free of charge via the Internet at http://pubs.acs.org/.

AUTHOR INFORMATION

Corresponding Author

*E-mail hdu@stevens.edu (H.D.) or ssukhish@stevens.edu (S.S.).

ACKNOWLEDGMENT

This research project has been supported by the Defense Advanced Research Projects Agency through Grant N66001-09-1-2076.

REFERENCES

(1) Kneipp, K.; Wang, Y.; Kneipp, H.; Perelman, L. T.; Itzkan, I.; Dasari, R. R.; Feld, M. S. *Phys. Rev. Lett.* **1997**, *78*, 1667–1670.

(2) Nie, S.; Emory, S. R. *Science* **1997**, *275*, 1102–1106.

(3) Campion, A.; Kambhampati, P. *Chem. Soc. Rev.* **1998**, *27*, 241–250.

(4) Lee, P. C.; Meisel, D. *J. Phys. Chem.* **1982**, *86*, 3391–3395.

(5) Hulteen, J. C.; Van Duyne, R. P. *J. Vac. Sci. Technol. A* **1995**, *13*, 1553–1558.

(6) Chan, S.; Kwon, S.; Koo, T. W.; Lee, L. P.; Berlin, A. A. *Adv. Mater.* **2003**, *15*, 1595–1598.

(7) Wang, H.; Levin, C. S.; Halas, N. J. *J. Am. Chem. Soc.* **2005**, *127*, 14992–14993.

(8) Qin, L.; Zou, S.; Xue, C.; Atkinson, A.; Schatz, G. C.; Mirkin, C. A. *Proc. Natl. Acad. Sci. U.S.A.* **2006**, *103*, 13300–13303.

(9) Lee, S. J.; Morrill, A. R.; Moskovits, M. *J. Am. Chem. Soc.* **2006**, *128*, 2200–2201.

(10) Ko, H.; Singamaneni, S.; Tsukruk, V. V. *Small* **2008**, *4*, 1576–1599.

(11) Ko, H.; Chang, S.; Tsukruk, V. V. *ACS Nano* **2009**, *3*, 181–188.

(12) Han, Y.; Tan, S.; Khaing, Oo, M. K.; Pristinski, D.; Sukhishvili, S.; Du, H. *Adv. Mater.* **2010**, *22*, 2647–2651.

(13) Chang, S.; Combs, Z. A.; Gupta, M. K.; Davis, R.; Tsukruk, V. V. *ACS Appl. Mater. Interfaces* **2010**, *2*, 3333–3339.

(14) Kahl, M.; Voges, E. *Phys. Rev. B* **2000**, *61*, 14078–14088.

(15) Banholzer, M. J.; Millstone, J. E.; Qin, L.; Mirkin, C. A. *Chem. Soc. Rev.* **2008**, *37*, 885–897.

(16) Yu, L.; Liu, G. L.; Kim, J.; Mejia, Y. X.; Lee, L. P. *Nano Lett.* **2005**, *5*, 119–124.

(17) Zhang, X.; Zhao, J.; Whitney, A. V.; Elam, J. W.; Van Duyne, R. P. *J. Am. Chem. Soc.* **2006**, *128*, 10304–10309.

(18) Haynes, C. L.; Van Duyne, R. P. *J. Phys. Chem. B* **2003**, *107*, 7426–7433.

(19) McFarland, A. D.; Young, M. A.; Dieringer, J. A.; Van Duyne, R. P. *J. Phys. Chem. B* **2005**, *109*, 11279–11285.

(20) Deng, X.; Braun, G. B.; Liu, S.; Sciortino, P. F., Jr.; Koefer, B.; Tombler, T.; Moskovits, M. *Nano Lett.* **2010**, *10*, 1780–1786.

(21) Lok, C. N.; Ho, C. M.; Chen, R.; He, Q. Y.; Yu, W. Y.; Sun, H.; Tam, P. K. H.; Chiu, J. F.; Che, C. M. *J. Biol. Inorg. Chem* **2007**, *12*, 527–534.

(22) Ivanova, O. S.; Zamborini, F. P. *J. Am. Chem. Soc.* **2009**, *132*, 70–72.

(23) Yin, Y.; Li, Z. Y.; Zhong, Z.; Gates, B.; Xia, Y.; Venkateswaran, S. *J. Mater. Chem.* **2002**, *12*, 522–527.

(24) Henglein, A. *Chem. Mater.* **1998**, *10*, 444–450.

(25) Henglein, A. *J. Phys. Chem.* **1993**, *97*, 5457–5471.

(26) Qi, H.; Alexson, D.; Glembocki, O.; Prokes, S. M. *Nanotechnology* **2010**, *21*, 215706.

(27) Pettenkofer, C.; Eickmans, J.; Ertürk, Ü.; Otto, A. *Surf. Sci.* **1985**, *151*, 9–36.

(28) Erol, M.; Han, Y.; Stanley, S. K.; Stafford, C. M.; Du, H.; Sukhishvili, S. *J. Am. Chem. Soc.* **2009**, *131*, 7480–7481.

(29) Khan, M. A.; Hogan, T. P.; Shanker, B. *J. Raman Spectrosc.* **2008**, *39*, 893–900.

(30) Waterhouse, G. I. N.; Bowmaker, G. A.; Metson, J. B. *Appl. Surf. Sci.* **2001**, *183*, 191–204.

(31) Carlisle, C. I.; Fujimoto, T.; Sim, W. S.; King, D. A. *Surf. Sci.* **2000**, *470*, 15–31.

(32) Jayadevan, K. P.; Kumar, N. V.; Mallya, R. M.; Jacob, K. T. *J. Mater. Sci.* **2000**, *35*, 2429–2434.

(33) Suzuki, R. O.; Ogawa, T.; Ono, K. *J. Am. Ceram. Soc.* **1999**, *82*, 2033–2038.

(34) Bomben, K. D.; Moulder, J. F.; Sobol, P. E.; Stickle, W. F. *Handbook of X-ray Photoelectron Spectroscopy*, 1st ed.; Perkin-Elmer: Eden Prairie, MN, 1992.

(35) Kaushik, V. K. *J. Electron Spectrosc. Relat. Phenom.* **1991**, *56*, 273–277.

(36) Bielmann, M.; Schwaller, P.; Ruffieux, P.; Gröning, O.; Schlapbach, L.; Gröning, P. *Phys. Rev. B* **2002**, *65*, 235431.

(37) Bukhtiyarov, V. I.; Kondratenko, V. A.; Boronin, A. I. *Surf. Sci. Lett.* **1993**, *293* (1−2), L826–L829.

(38) Bukhtiyarov, V. I.; Boronin, A. I.; Oschepkova, M. P.; Savchenko, V. I. *React. Kinet. Catal. Lett.* **1989**, *39*, 21–26.

(39) Zemlyanov, D. Y.; Savinova, E.; Scheybal, A.; Doblhofer, K.; Schlögl, R. *Surf. Sci.* **1998**, *418*, 441–456.

(40) NIST X-ray photoelectron spectroscopy database: http://srdata.nist.gov/xps/Default.aspx.

(41) Gu, B.; Tio, J.; Wang, W.; Ku, Y. K.; Dai, S. *Appl. Spectrosc.* **2004**, *58*, 741–744.

(42) Wang, W.; Ruan, C.; Gu, B. *Anal. Chim. Acta* **2006**, *567*, 121–126.

(43) Goulet, P. J. G.; Dos Santos, D. S., Jr.; Alvarez-Puebla, R. A.; Oliveira, O. N., Jr.; Aroca, R. F. *Langmuir* **2005**, *21*, 5576–5581.

(44) Aroca, R. F.; Goulet, P. J. G.; Dos Santos, D. S., Jr.; Alvarez-Puebla, R. A.; Oliveira, O. N., Jr. *Anal. Chem.* **2005**, *77*, 378–382.

(45) Li, X.; Xu, W.; Zhang, J.; Jia, H.; Yang, B.; Zhao, B.; Li, B.; Ozaki, Y. *Langmuir* **2004**, *20*, 1298–1304.

(46) Schmitt, J.; Machtle, P.; Eck, D.; Mohwald, H.; Helm, C. A. *Langmuir* **1998**, *15*, 3256–3266.

(47) Burstein, E.; Chen, Y. J.; Chen, C. Y.; Lundquist, S.; Tosatti, E. *Solid State Commun.* **1979**, *29*, 567–570.

(48) Gersten, J. I.; Birke, R. L.; Lombardi, J. R. *Phys. Rev. Lett.* **1979**, *43*, 147–150.

(49) Pemberton, J. E.; Coria-Garcia, J. C.; Hoff, R. L. *Langmuir* **1987**, *3*, 150–159.

(50) Smith, E.; Dent, G. *Modern Raman Spectroscopy: A Practical Approach*; Wiley : Chichester, U.K., 2005.

(51) Schatz, G. C.; Young, M. A.; Duyne, R. P. V. In *Surface-Enhanced Raman Scattering—Physics and Applications*; Kneipp, K., Moskovits, M., Kneipp, H., Eds.; Springer: New York, 2006; pp 19−46.

(52) Murray, C. A. *J. Opt. Soc. Am. B* **1985**, *2*, 1330–1339.

(53) Guy, A. L.; Bergami, B.; Pemberton, J. E. *Surf. Sci.* **1985**, *150*, 226–244.

(54) Takayanagi, K.; Kolb, D. M.; Kambe, K.; Lehmpfuhl, G. *Surf. Sci.* **1980**, *100*, 407–422.

(55) Le Ru, E. C.; Blackie, E.; Meyer, M.; Etchegoin, P. G. *J. Phys. Chem. C* **2007**, *111*, 13794–13803.

(56) Popkirov, G. S.; Burmeister, M.; Schindler, R. N. *J. Electroanal. Chem.* **1995**, *380*, 249–254.

(57) Brus, L. *Acc. Chem. Res.* **2008**, *41*, 1742–1749.

(58) Auge, A.; Weddemann, A.; Vogel, B.; Wittbracht, F.; Hütten, A. Proceedings of the Comsol Conference, Milan, Italy, 2009.